



# Improved power generation using nitrogen-doped 3D graphite foam anodes in microbial fuel cells

Wei Guo<sup>1</sup> · Shujun Chao<sup>1</sup> · Qianjiang Chen<sup>2</sup>

Received: 17 July 2019 / Revised: 4 September 2019 / Accepted: 9 September 2019 / Published online: 18 September 2019  
© Springer-Verlag GmbH Germany, part of Springer Nature 2019

## Abstract

The properties of the anode material and structure are critical to the microbial growth and interfacial electron transfer between the biofilm and the anode. In this paper, we prepared the nitrogen-doped 3D expanded graphite foam (NEGF) by simple, rapid and inexpensive methods of liquid nitrogen expansion and hydrothermal treatment from commercial graphite foil (GF). X-ray photoelectron spectroscopy confirmed the success of nitrogen doping on expanded graphite foam (EGF). Using cyclic voltammetry and electrochemical impedance spectroscopy, the NEGF and EGF electrode exhibited increased electrochemical active surface area and fast interfacial electron transfer ability than that of pristine GF, and NEGF electrode performed even better. Scanning electron microscopy revealed that NEGF and EGF possessed graphene-like structure and large surface area. MFCs equipped with NEGF or EGF anodes, respectively, achieved maximum power density of 0.739 and 0.536 W m<sup>-2</sup>, which was about 17.4 and 12.6 times larger than that of MFCs with GF anodes (0.0451 W m<sup>-2</sup>). The anode and cathode polarization curves further confirmed that the different anode other than the cathode was responsible for the advanced performance of MFCs. The morphology of the biofilm on three kinds of anodes proved the densest biofilm formed on NEGF anode. All the results indicated the synergistic effect of 3D graphene-like structure and N-doped surface on the performance of MFCs, which might provide special insights into designing simple and efficient route for anode construction to achieve promising electricity generation.

**Keyword** Microbial fuel cells · Anode · Three dimensional graphite · Nitrogen doping

## Introduction

Microbial fuel cells (MFCs) convert chemical energy to electrical energy via the catalysis of electroactive microorganisms. Recently, MFCs have gained increasing attention because this technique provides a dual benefit of generating biomass-based energy and wastewater treatment simultaneously [1–3]. However, the relatively low power density compared to other energy sources hinders their further application. The anode materials and structure have been considered as one of the most important factors in improving the performances of MFCs by influencing the growth and

activities of microbes as well as the electron transfer rates from the microbial to the anode [4, 5]. Therefore, developing effective anode becomes one of the research hot spots for enhancing the power density of MFCs.

The optimal anode must have good biocompatibility, excellent conductivity, big specific surface area, which are benefit for promoting microbial adhesion and interfacial electron transfer. In addition to these properties, the ideal anode should also be readily available, low-cost, mechanically and chemically stable [6, 7]. Metallic anodes, such as stainless-steel, have excellent conductivity, good mechanical strength and low cost, but poor biocompatibility. Many researchers have tried to improve the biocompatibility of metallic electrodes through surface modification with excellent biocompatibility materials [8]. These types of electrodes can greatly improve the power production of MFCs, but their preparation processes are usually complex and thus increase the cost. Compared to the metallic anodes, carbon-based materials, such as carbon cloth or carbon paper, have been widely used as anode due to their remarkable

✉ Wei Guo  
cligw@163.com

<sup>1</sup> Department of Chemistry, Xinxiang Medical University, Xinxiang 453003, People's Republic of China

<sup>2</sup> Grade 2017, Clinical Pharmacy, School of Pharmacy, Xinxiang Medical University, Xinxiang 453003, People's Republic of China

biocompatibility, conductivity, stability and low cost [9–12]. However, these materials suffer relatively limited surface areas and relatively small electrochemical activities, retarding the interaction between microorganisms and the anodes [13, 14]. One effective method for addressing these challenges is to design and fabricate 3D carbon-based materials [15]. So far, several latest papers have reported that the MFCs equipped with 3D carbon anodes showed improved performance than that of MFCs with plain carbon anodes under the same experimental conditions. Xie et al. proposed high-performance MFCs with 3D anodes designed by coating macroscale porous substrates, such as textiles and sponges, with carbon nanotubes or graphene nanosheets [16–18]. Yong et al. fabricated MFCs anodes based on polyaniline hybridized three-dimensional graphene with nickel foam substrates. It impressively outperformed the commonly used carbon cloth owing to the higher bacterial biofilm loading and higher EET efficiency [19]. Wang et al. reported the fabrication of flexible MFCs anodes by coating nickel foam with reduced graphene oxide sheets, showing great promise for improving the power generation of MFC devices [20]. Lu et al. and Yuan et al., respectively, prepared high-performance 3D materials with high specific surface area and good biocompatibility by carbonizing natural biomass loofah sponge and silk cocoon, and used as the anodes to improve the power output of MFCs [21, 22]. Chen et al. proposed layered corrugated carbon, which is produced from the carbonization of corrugated cardboard, as an inexpensive and high-performance electrode material [23]. But carbonization is usually a high-temperature process, which need higher energy cost and has higher requirements for the equipment. Bian et al. firstly utilized anodes with 3D porous carbon structure via 3D printing technique and controlled carbonization process. Compared to the 2D plain anode materials, 3D anodes showed significantly improved electrochemical performance, which were attributed to their larger surface area, better mass transfer, excellent biocompatibility and enhanced bacterial adhesion [24]. Zhao et al. reported that MFCs with Pt nanoparticles decorated three dimensional graphene aerogel as anode materials and realized a maximum power density of  $1.46 \text{ W m}^{-2}$  [25].

However, these materials suffer sophisticated preparation process, time-consuming, difficulty in preparing large-scale materials and high cost. To reduce the cost and simplify the preparation, it is highly necessary to develop an inexpensive, easy and fast method to prepare 3D carbon-based materials. Zhang et al. fabricated 3D graphite foam from commercial graphite foil upon liquid nitrogen expansion process [26], which was based on the flash gasification of liquid nitrogen molecules that penetrated into inter-layer space between graphite nanoflakes in ethanol at room temperature. This method is a complete physical process, it can preserve the excellent conductivity of graphite and

it is easy, rapid, inexpensive and large scalable. It would be a promising method to prepare 3D carbon-based materials. Chen et al. further prepared thermal treated expanded graphite foil. They used thermal treated expanded graphite foil and expanded graphite foil as the anodes of MFCs and achieved significantly higher power density, which were 6.5 and 9.5 times higher than that of MFCs with pristine graphite foil anodes [27].

Recently, doping of nitrogen on the anode surface is demonstrated to be an effective way to improve the power output of MFCs. N-doping might lead to enhanced microbial attachment on the surface of electrodes and increased biocatalytic activity due to their good biocompatibility and unique electronic properties [28, 29]. Bi et al. prepared three-dimensional nitrogen-doped porous carbons (N/PCs) and applied as anode materials of MFCs, whose maximum power density were approximately twice higher than that of MFCs with commercial carbon cloth anodes [30]. Yang et al. synthesized the highly conductive and hierarchical porous nitrogen-doped graphene aerogel (N-GA) as the outstanding anodes. The 3D N-GA anodes showed great promise for improving the power density of MFCs [15]. Wu et al. developed a hierarchically porous nitrogen-doped CNTs/reduced graphene oxide composite for MFC anode. The maximum power density achieved with the N-CNTs/rGO anode was 8.9 times compared with that of carbon cloth anode and higher than that of CNTs/rGO anode [31]. Mohamed et al. investigated three different strategies for doping superficial nitrogen groups on the surfaces of carbon cloth and carbon paper. The results showed that the power densities were significantly affected by the surface modification and highlighted the significance of anode surface modification for enhancing MFC performance [32].

Based on the brilliant advantages of 3D carbon-based materials and nitrogen-doping surface modification, in this paper, we fabricated nitrogen-doped 3D expanded graphite foam (NEGF) by liquid nitrogen expansion and hydrothermal treatment using ammonia solution. XPS proved the successful doping of nitrogen. The electrochemical performances of pristine GF, EGF and NEGF had been studied with the aid of cyclic voltammetry (CV) and electrochemical impedance spectroscopy (EIS). Both EGF and NEGF electrodes showed increased electrochemical active surface area and electron transfer ability than that of GF, and NEGF electrode exhibited even better performance. Morphology study revealed that EGF or NEGF possessed graphene-like structure and large surface area. Consequently, the usage of NEGF as anode enabled improved performance in MFCs in terms of higher output power density and much denser biofilm, which was probable result from the synergistic effect of 3D graphene-like structure and N-doping chemical surface.

## Materials and methods

### Chemicals

Carbon paper and DuPont Nafion 117 proton exchange membrane (PEM) were purchased from Shanghai Hesen Engineering Co. Ltd. Carbon papers (3 × 3 cm) were used as cathodes, and were pretreated first by soaking in acetone for 4 h to remove organic matters on the surface, then soaking in 1 mol L<sup>-1</sup> HCl and 1 mol L<sup>-1</sup> NaOH, respectively, for 24 h to wipe out impurities. In order to prevent the Nafion 117 membranes swelling by water when they were placed in the MFCs compartment, the membranes were pretreated by boiling in H<sub>2</sub>O<sub>2</sub> (30%, v/v) and deionized water for 0.5 h in order, followed by soaking in 0.5 M H<sub>2</sub>SO<sub>4</sub> for 1 h and then deionized water for 1 h. Finally the membranes were stored in deionized water prior to use [33]. All chemicals were of analytical reagent grade and used without further purification. Deionized water was used throughout the study.

### Electrode preparation

The expanded graphite foil (EGF) was constructed from commercial graphite foil (GF) through an easy and fast expansion process according to literatures [26, 27]. Prior to use, the GF was cut into small pieces, a size of 3 × 3 cm for anodes of MFCs, and a size of 1 × 2 cm for CV and EIS measurements. The GF was pretreated as follows, firstly cleaned by soaking in pure acetone for 4 h to remove adsorbed organic contaminations and then successively immersed in 0.1 mol L<sup>-1</sup> HCl, 0.1 mol L<sup>-1</sup> NaOH and deionized water for 24 h to wipe out possible impurities. At last, the GF was dried at 60 °C for 2 h.

After pretreatment, the GF was first soaked in liquid nitrogen solution for 30 min aiming to let the liquid nitrogen molecules penetrated into interlayer space of GF, and then the GF was quickly transferred from the liquid nitrogen solution to absolute ethanol at room temperature, result in volume expansion in an instant triggered by gasification of liquid nitrogen in interlayer space of GF, thus producing expanded graphite foil (EGF). Then the EGF was fully washed with distilled water and dried at 60 °C for 2 h. During the processes, most ethanol would be removed from the as-prepared EGF. As shown in Fig. 1, the thickness of EGF is about 12 mm, which is about 12 times larger than that of commercial graphite foil (1 mm).

To prepare NEGf [32], the EGF was immersed in 20 mL of the 25–28% ammonia solution in a teflon-lined stainless steel autoclave and maintained at 180 °C for 3 h in a muffle furnace. The autoclave was left to cool inside

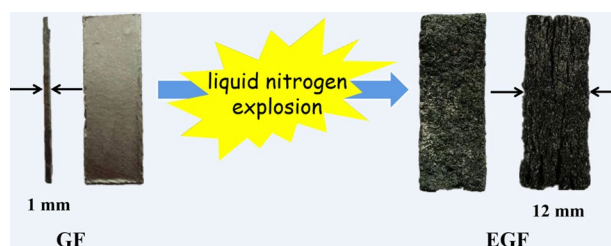


Fig. 1 Photographs of GF and EGF

the furnace, and then the as-prepared NEGf was washed fully with distilled water and dried at 60 °C for 2 h before use in the MFCs. As for NEGf, during the high-temperature treatment and the following washing and drying process, residual ethanol was believed to be further removed.

### Construction and operation of MFCs

A two-chambered MFC made of perspex material was consisted of an anode chamber and a cathode chamber, each with a volume of 140 mL. Proton exchange membrane (PEM) was sandwiched between the two chambers and held together by external stainless screws. Rubber gaskets were used to secure the sealing between the perspex material and the membrane. For comparison, the anodes were GF, EGF or NEGf and all the cathodes were carbon papers. The anode and the cathode were connected with an external resistance of 1000 Ω. 100 mmol L<sup>-1</sup> K<sub>3</sub>[Fe(CN)<sub>6</sub>] in 50 mmol L<sup>-1</sup> phosphate buffer solution (PBS, pH 7.0) was used as the electron acceptors.

Anaerobic sludge collected from a local wastewater treatment plant (Xinxiang, China) was inoculated as the anodic inoculums of MFCs. A cultivation solution added to the anode chamber for bacterial growth contained 1 g L<sup>-1</sup> sodium acetate, 50 mmol L<sup>-1</sup> PBS (pH 7.0) containing (per liter deionized water): 3.32 g NaH<sub>2</sub>PO<sub>4</sub>·2H<sub>2</sub>O, 10.32 g Na<sub>2</sub>HPO<sub>4</sub>·12H<sub>2</sub>O, 0.13 g KCl, 0.31 g NH<sub>4</sub>Cl, 12.5 mL vitamins and 12.5 mL mineral solution. The inoculated anaerobic sludge was set to 25% (volume ratio) of the whole anode chamber. All MFCs were operated in batch cycle mode. When the output voltage decreased below 50 mV, the anode solution was replaced by fresh cultivation solution which had been continuously flushed with N<sub>2</sub> gas for 15 min. All MFC experiments were conducted at 30 ± 1 °C in a constant temperature room. As the biological fluctuation of the anaerobic sludge and other MFCs experimental conditions could affect the results, three parallel groups of experiments were performed, and their average values of the results were taken.

## Characterization

A Versa STAT3 (Princeton Applied Research) electrochemical workstation was used for electrochemical measurements including cyclic voltammetry (CV) and electrochemical impedance spectroscopy (EIS). A regular three-electrode cell was used with a GF, EGF or NEGF as the working electrode, a saturated calomel electrode (SCE) as the reference electrode, and a platinum wire as the counter electrode. EIS measurements were performed in the frequency range from 100 kHz to 0.01 Hz with sinusoidal perturbation of 5 mV amplitude under open circuit potential, and the obtained data were analyzed using ZSimpWin 3.10 software.

The voltage of the MFCs was measured every 30 min with a data recorder. Polarization curves were obtained by changing external circuit resistance from 10,000 to 50  $\Omega$  when the voltage reached a steady and repeatable state. The current density,  $I_A$  ( $A\ m^{-2}$ ) and the power density,  $P_A$  ( $W\ m^{-2}$ ) of the system can be calculated using the formulas:

$$I_A = \frac{V}{R \cdot A} \quad (1)$$

$$P_A = \frac{V^2}{R \cdot A}, \quad (2)$$

where  $V$  (V) is the cell voltage,  $R$  ( $\Omega$ ) is the external resistances and  $A$  ( $m^2$ ) is the projected area of the anode.

The surface morphology of GF, EGF or NEGF was observed using a SU-8000 field emission scanning electron microscopy (FESEM) (HITACHI, Japan). X-ray photoelectron spectroscopy (XPS) was performed on an X-ray photoelectron spectrometry (ESCALAB 250Xi, USA).

The surface morphology of the biofilms on various anodes after worked for about 90 days in MFCs were observed by a JSM-7800F field emission scanning electron microscopy (JEOL, Japan). The pretreatment was carried out as follows: (1) The samples were collected by cutting off small pieces of GF, EGF or NEGF anodes using sterile scissors. (2) The samples were immediately fixed in a 2.5% glutaraldehyde (commercial 25% glutaraldehyde solution diluted with 2 mol  $L^{-1}$  PBS) overnight at 4  $^{\circ}C$ . (3) The samples were dehydrated by successively immersing in 30%, 50%, 70%, 80%, 90% ethanol solution and 100% ethanol, each for 10 min. (5) The samples were immersed in tertiary butanol twice, each for 10 min. (6) The samples were vacuum freeze dried. (7) The samples were finally coated with Au before SEM observation.

## Results and discussion

### Physicochemical properties of GF, EGF and NEGF

#### Morphology study

The morphology of the GF, EGF and NEGF was investigated by SEM and the results were shown in Fig. 2. The raw material GF possessed compact laminated structure with relatively smooth surface (Fig. 2a, b). In contrast, after “liquid nitrogen explosion”, the flash gasification of liquid nitrogen in interlayer space between graphite nanoflakes resulted in a fast expansion of GF, generating greatly-crumpled graphite nanoflakes on the surface of the EGF (Fig. 2c). And at higher magnification, graphene-like structure with typically wrinkled graphene sheet could be observed on the surface of the crumpled graphite nanoflakes (Fig. 2d, e). It was clear shown that the graphene-like structure and the rough surface of EGF provided much larger specific surface area compared to that of GF. Therefore, it would be beneficial to the adsorption and growth of specific microbial on the anode surface, implying a good performance of MFC. There was not significant morphology difference between EGF and NEGF, revealed that the nitrogen doping treatment did not cause significant change on the morphology of EGF (Fig. 2f–h).

#### Characterization of the chemical composition

X-Ray photoelectron spectroscopy (XPS) analysis was then employed to probe the elemental composition of the material surface. The success of nitrogen doping on EGF was confirmed by XPS spectra. Figure 3a, b compared the XPS survey spectra of EGF and NEGF. The spectrum of NEGF showed a small peak at  $\approx 400$  eV (inset plot of Fig. 3a), which could be assigned to N 1 s, while no obvious peak could be observed in the spectrum of EGF at the same binding energy (inset plot of Fig. 3b). The N 1 s peak of NEGF (inset plot of Fig. 3a) centered at 399.7 eV was consistent with the binding energy reported for the presence of N BE  $\approx 400$  eV) atoms on the surface of nitrogen doped carbon-based materials. Figure 3c exhibited the high-resolution XPS spectrum of N 1 s for the NEGF. The N 1 s peak could be fitted to two peaks located at 399.2 and 400.6 eV, corresponding to pyrrolic N and graphitic N [34]. The XPS results confirmed the success of nitrogen doping on EGF.

#### Electrochemical analysis

The electrochemical behaviors of the GF, EGF and NEGF electrodes were evaluated by cyclic voltammetry (CV) in 5 mmol  $L^{-1}$   $K_3[Fe(CN)_6]$  (used as the redox

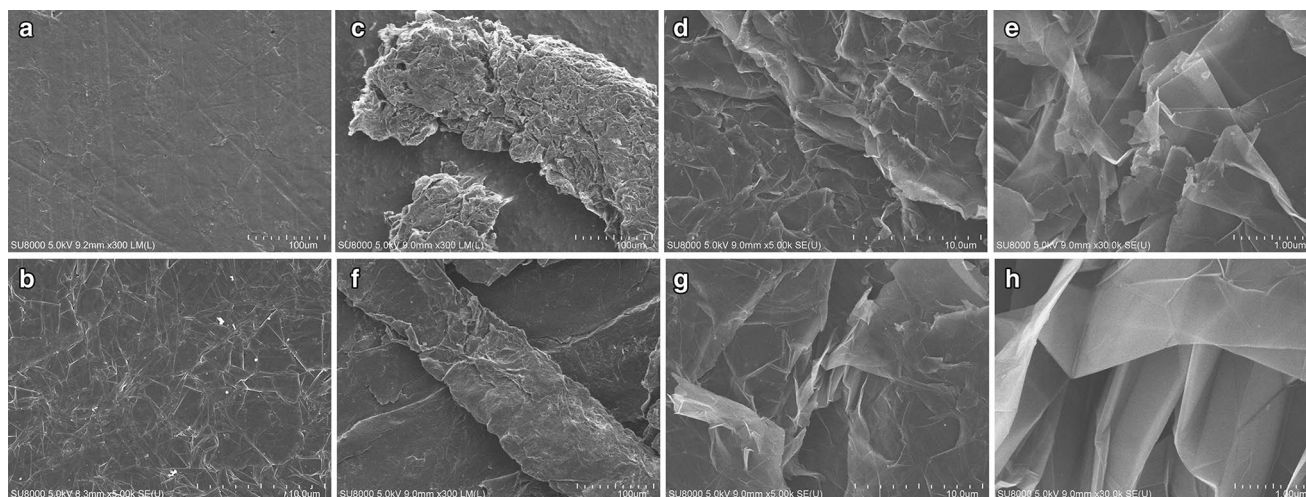


**Fig. 2** SEM images of GF (a, b), EGF (c–e), and NEGF (f–h)

electrochemical probe) containing  $0.1 \text{ mol L}^{-1}$  KCl. As shown in Fig. 4a, a pair of well-defined, nearly reversible reduction–oxidation peaks at  $0.17 \text{ V}$  vs. SCE was observed on all kinds of electrodes, which correspond to the  $[\text{Fe}(\text{CN})_6]^{3-}/[\text{Fe}(\text{CN})_6]^{4-}$  redox couple. Obviously, in comparison with the raw material GF electrode, both the anodic ( $i_{pa}$ ) and cathodic peak currents ( $i_{pc}$ ) on the EGF and NEGF electrode were remarkably enhanced. Furthermore, compared to EGF, the peak currents on NEGF were even higher. NEGF and EGF revealed a cathodic peak current of  $11.49$  and  $9.46 \text{ mA}$  at a scan rate of  $5 \text{ mV s}^{-1}$ , which is about  $18.3$  and  $15.1$  times higher than those of GF, respectively.

Furthermore, the electrochemical active surface area (EASA) responses the area with conductive path to transfer electrons in the electrode surface. The EASA of GF, EGF and NEGF was obtained by measured the reduction peak currents of CV and calculated based on the Randles–Sevcik equation:

$$i_{pc} = 2.69 \times 10^{-5} n^{3/2} A D^{1/2} c v^{1/2}, \quad (3)$$

where,  $i_{pc}$  (A) is the reduction peak current,  $n$  is the number of electrons transferred in the electrochemical reaction ( $n = 1$ ),  $A$  ( $\text{cm}^2$ ) is the electrochemical active surface area (EASA),  $D$  ( $\text{cm}^2 \text{ s}^{-1}$ ) is the diffusion coefficient of  $\text{K}_3[\text{Fe}(\text{CN})_6]$  ( $D \approx 6.3 \times 10^{-6} \text{ cm}^2 \text{ s}^{-1}$ ),  $c$  ( $\text{mol mL}^{-1}$ ) is the concentration of  $\text{K}_3[\text{Fe}(\text{CN})_6]$  ( $5 \times 10^{-6} \text{ mol mL}^{-1}$ ) and  $v$  is the scan rate of the CV (from  $0.005$  to  $0.1 \text{ V s}^{-1}$ ).

The Randles–Sevcik plots revealed that  $i_{pc}$  was linearly related to  $v^{1/2}$ , and the EASA can be calculated from the slope of the linear fitting line. The EASA were  $3.17 \pm 1.53$ ,  $51.2 \pm 5.3$ , and  $61.3 \pm 4.4 \text{ cm}^2$  for GF, EGF and NEGF, respectively (Fig. 4b). Obviously, the NEGF and EGF possessed significantly larger EASA than that of GF, increased

by about  $20$  and  $17$  fold. The result demonstrated that much larger active reaction area and more electrochemical active sites could be provided for electron transfer after “nitrogen explosion” and surface N-doping.

Electrochemical impedance spectroscopy (EIS) technique was employed to further study the electrode interfacial resistance of GF, EGF and NEGF. Figure 5 showed the impedance spectra in the form of Nyquist diagrams for three kinds of electrodes in  $10 \text{ mmol L}^{-1} \text{ K}_3[\text{Fe}(\text{CN})_6]$  containing  $0.1 \text{ mol L}^{-1}$  KCl (used as the electrochemical probe), where the inset depicted the high-frequency part of the result. It is known that the diameter of the semicircle impedance curve over high frequencies corresponds to the charge transfer resistance ( $R_{ct}$ ) of the electrochemical reaction at electrode/electrolyte interface, which reveals the charge transfer kinetics of the redox electrochemical probe at the electrode interface [35]. The  $R_{ct}$  values for GF, EGF and NEGF were estimated to be  $17.8$ ,  $2.91$  and  $1.84 \Omega \text{ cm}^2$ , respectively. Firstly, all of the electrodes showed the relatively small value of  $R_{ct}$ , indicating a fast charge transfer rate between electrode and electrolyte, due to the excellent conductivity of carbon-based materials. Furthermore, The  $R_{ct}$  of EGF and TEGF were obviously smaller than that of GF, the apparent reduction in  $R_{ct}$  values implied that the liquid nitrogen expansion process and the resulting graphene-like structure significantly reduced the charge transfer resistance and realized a faster electrochemical reaction between the electrode and electrolyte. Moreover, the straight line region is characteristic of a diffusion-limiting step in an electrochemical process [35]. It could be seen that the straight line region over low frequency of the EGF and NEGF were significantly smaller than that of GF, indicating more proper accommodations provided by EGF and NEGF electrodes for reactants to access the

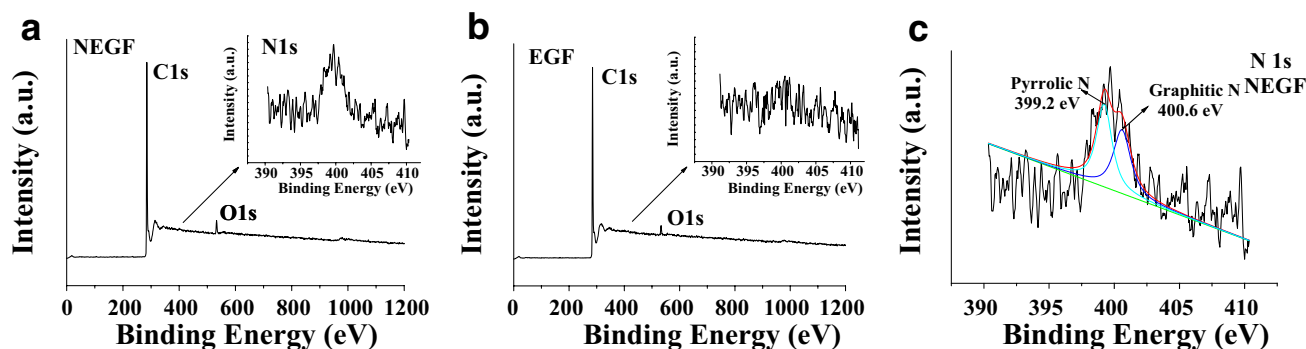
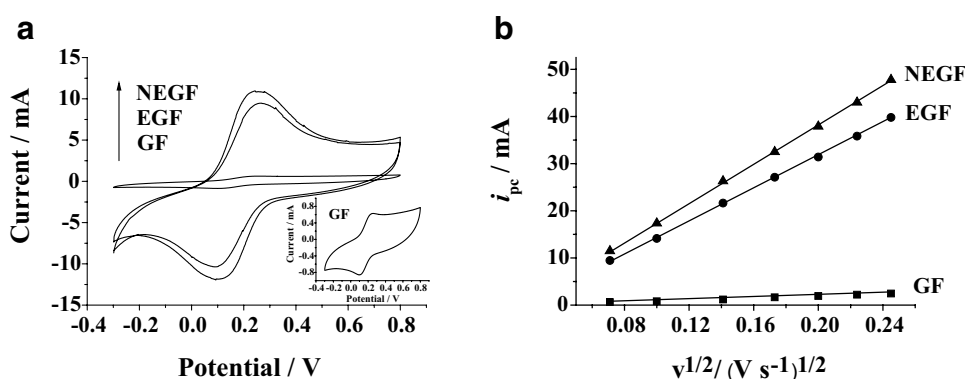


**Fig. 3** XPS spectra of NEGF (a) and EGF (b) and the high-resolution spectra of N 1 s for the NEGF (c)

**Fig. 4** a CV curves of GF, EGF and NEGF as working electrodes in 5 mmol L<sup>-1</sup> K<sub>3</sub>[Fe(CN)<sub>6</sub>] solution containing 0.1 mol L<sup>-1</sup> KCl at a scan rate of 5 mV s<sup>-1</sup>. b Relationship between square root of scanning rate and the reduction peak current for the GF, EGF and NEGF electrodes at scan rates of 5, 10, 20, 40, 60, 80, and 100 mV s<sup>-1</sup>



reaction centers and improved diffusion of electrolyte toward the surface of the electrode [36].

## Performances of MFCs with various anodes

### Electricity generation

The performances of GF, EGF and NEGF anode-based MFCs were evaluated by measuring the output voltage over 1000 Ω external resistance. Figure 6a showed representative cycles. MFCs equipped with NEGF and EGF anodes achieved much better performance than that with pristine GF anodes. Firstly, the GF-MFCs produced a peak cell voltage of 0.357 ± 0.032 V, while the NEGF-MFCs and EGF-MFCs produced higher maximum voltage of 0.664 ± 0.052 V and 0.620 ± 0.041 V, increased by nearly 86.0% and 73.7%, respectively; Secondly, the start-time for reaching the initial maximum stable voltage was about 500 h and 680 h for NEGF-MFCs and EGF-MFCs, compared to nearly 1000 h for GF-MFCs, shortened by 50% and 32%, respectively.

Based on the morphology studies, we deduced that the NEGF and EGF anodes afforded the increased specific surface area for improved biofilm formation, and the “liquid nitrogen explosion” process formed graphene-like structure, which exposed more graphene edges, the

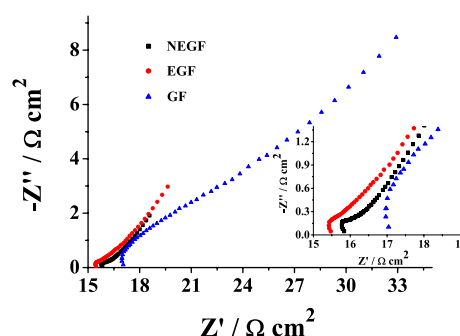


**Fig. 5** Nyquist plots of GF, EGF and NEGF as working electrodes in 10 mmol L<sup>-1</sup> K<sub>3</sub>[Fe(CN)<sub>6</sub>] solution containing 0.1 mol L<sup>-1</sup> KCl. The insert illustrated the high-frequency part of the result

electron transfer between bacteria and electrode was faster on the graphite edge than that on the basal plane [37], thus resulting in better performance in terms of voltage generation. Furthermore, NEGF-MFCs showed even better performance than EGF-MFCs. As the roughness of EGF and NEGF was similar and they had the comparable specific surface area, it could be speculated that the NEGF anode with superficial N-doping surface might induce the enhanced adhesion of microorganisms on the anode surface and simultaneously reduce the overpotential with

increasing biocatalytic activity [30, 38], leading to even better performance than EGF-MFCs. Another possible reason we should notice might be the different amount of residual ethanol in EGF and NEGF. During the preparation process of EGF and NEGF, ethanol was used to gasify liquid nitrogen. Although most of the ethanol was believed to be removed during the washing and drying process, trace amount of ethanol might still be residue in EGF and NEGF. According to the relevant literatures [27, 39], the residual ethanol might have adverse effects on the bioelectricity production. As the preparation of NEGF included high-temperature treatment process, so it was believed that residual ethanol is further removed from NEGF. That is less residual ethanol would exist in NEGF than that in EGF, which might be another possible reason why NEGF-MFCs showed better performance than EGF-MFCs.

Figure 6 b showed the power density curves of the three types of MFCs with the external resistance varied from 10,000 to 50 Ω. The maximum power density of 0.739 and 0.536 W m<sup>-2</sup> was obtained in MFCs with NEGF and EGF anodes, respectively, which was about 17.4 and 12.6 times larger than that generated by

GF-MFCs (0.0451 W m<sup>-2</sup>). The results further verified that the explosion process and N-doping strategy indeed affected the performance of MFCs and improved the power output.

Furthermore, the individual electrode polarization behaviors were investigated to make clear whether the anode or the cathode played the more important role in promoting the power output of the MFCs. Results were depicted in Fig. 6c. It could be seen that the three types of MFCs presented similar cathode potential changing trend. It is understandable because the cathodes and the cathodic solution were the same for the three types of MFCs. It was worth noting that the anode polarization curves were different, pristine GF anode showed the largest slope, indicating the largest overpotential would be required for the bioelectrochemical reaction at high currents [40]. The lower anode overpotential with the NEGF and EGF anodes reflected the positive role played by the graphene-like structure and the N-doping surface in enhancing the bioelectroactivity of the anodes [14]. The results verified that the difference in the overall power output was mainly attributed to the difference of the anodes.

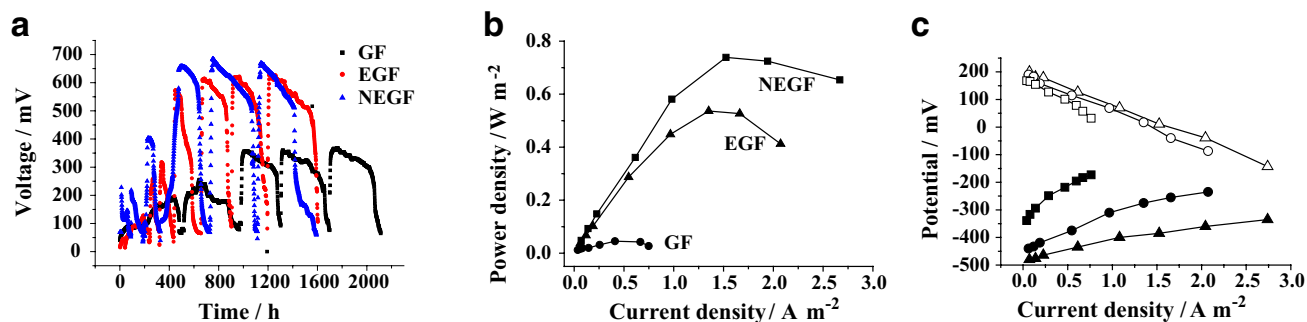


**Fig. 6** Performance of MFCs with GF, EGF and NEGF anodes: **a** cell voltage output as a function of time under 1000 Ω external resistance **b** power density curves **c** anode (solid symbol) and cathode (hollow

symbol) polarization curves (GF black square, EGF black circle, and NEGF black triangle)

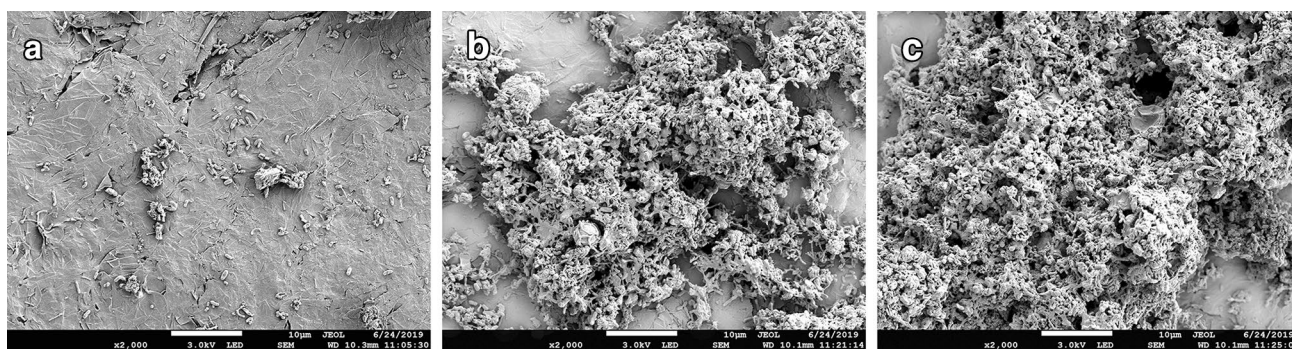


**Fig. 7** SEM images of the biofilm formed on the GF (a), EGF (b) and NEGF (c) anodes after worked nearly 90 days in MFCs

## Biofilm morphology study

The surface morphology of GF, EGF and NEGF anodes were observed by SEM after nearly 90 days of operation (Fig. 7). In case of GF, bacterial were sparsely distributed on the surface of the electrode (Fig. 6a). On the contrary, bacterial colonies can be easily seen on EGF (Fig. 7b) and NEGF (Fig. 7c). The observations confirmed that EGF and NEGF indeed promoted the bacteria adhesion and growth, which was attributed to the large specific surface area of the graphene-like structure. At the same time, even thicker biofilm was formed on the surface of NEGF. It is highly probably due to the N-doping on the surface of NEGF, which might give rise to an increased biocompatibility and form a suitable micro-environment for microbial growth. Therefore a much denser biofilm was formed on the surface of NEGF anode, and eventually helped to further improve the performance of MFCs [30].

## Conclusions

In summary, we have employed an easy, fast and effective method to prepare nitrogen-doped 3D expanded graphite foam (NEGF) from commercial graphite foil. The as-prepared NEGF showed increased surface area with graphene-like structure, nitrogen doping chemical surface and improved electrochemical activity, as supported by XPS, SEM, CV and EIS. MFCs with NEGF or EGF as anodes achieved enhanced performance, and MFCs with NEGF anodes performed even better. Compared to MFCs with GF anodes, the maximum power density of NEGF-MFCs ( $0.739 \text{ W m}^{-2}$ ) and EGF-MFCs ( $0.536 \text{ W m}^{-2}$ ) was about 17.4 and 12.6 times larger, respectively, and the start-time of NEGF-MFCs (500 h) and EGF-MFCs (680 h) shortened by 50% and 32%, respectively. Through our investigation we speculated that the advanced performance of MFCs with NEGF anodes was associated with the synergistic effect of unique graphene-like structure of the expanded graphite foil and the nitrogen doped surface, such as large specific surface area, excellent conductivity and the increased biocompatibility. All the advantages were beneficial to the attachment and growth of bacteria on the anode and to the improvement of the interfacial electron transfer from microbial to electrode. In all, the simple and efficient way of preparing N-doped 3D expanded graphite could introduce a promising choice for designing high-performance MFCs for practical application.

**Acknowledgements** The authors are grateful to the financial support from the National Natural Science Foundation of China (Grant No. 21601151) and the Scientific and Technological Research Projects of Henan Province, China (Grant No. 172102210449).

## Compliance with ethical standards

**Conflict of interest** There are no conflicts of interest to declare.

## References

1. Logan BE, Rabaey K (2012) Conversion of wastes into bioelectricity and chemicals by using microbial electrochemical technologies. *Science* 337:686–690
2. Li WW, Yu HQ, He Z (2014) Towards sustainable wastewater treatment by using microbial fuel cells-centered technologies. *Energy Environ Sci* 7:911–924
3. Zhao CE, Gai PP, Song RB, Chen Y, Zhang JR, Zhu JJ (2017) Nanostructured material-based biofuel cells: recent advances and future prospects. *Chem Soc Rev* 46:1545–1564
4. Sonawane JM, Yadav A, Ghosh PC, Adeloju SB (2017) Recent advances in the development and utilization of modern anode materials for high performance microbial fuel cells. *Biosens Bioelectron* 90:558–576
5. He Z, Liu J, Qiao Y, Li CM, Tan TTY (2012) Architecture engineering of hierarchically porous chitosan/vacuum-stripped graphene scaffold as bioanode for high performance microbial fuel cell. *Nano Lett* 12:4738–4741
6. Logan BE (2007) *Microbial fuel cells*. Wiley, New York
7. Wang RW, Yan M, Li HD, Zhang L, Peng BQ, Sun JZ, Liu D, Liu SQ (2018) FeS<sub>2</sub> nanoparticles decorated graphene as microbial fuel cell anode achieving high power density. *Adv Mater* 30:e1800618
8. Wu GM, Bao H, Xia Z, Yang B, Lei LC, Lia ZJ, Liu CX (2018) Polypyrrole/sargassum activated carbon modified stainless-steel sponge as high-performance and low-cost bioanode for microbial fuel cells. *J Power Sources* 384:86–92
9. Logan BE, Hamelers B, Rozendal RA, Schrorder U, Keller J, Freguia S, Aelterman P, Verstraete W, Rabaey K (2006) Microbial fuel cells: methodology and technology. *Environ Sci Technol* 40:5181–5192
10. Wang X, Cheng SA, Feng YJ, Merrill MD, Saito T, Logan BE (2009) Use of carbon mesh anodes and the effect of different pretreatment methods on power production in microbial fuel cells. *Environ Sci Technol* 43:6870–6874
11. Hidalgo D, Tommasi T, Bocchini S, Chiolerio A, Chiodoni A, Mazzarino I, Ruggeri B (2016) Surface modification of commercial carbon felt used as anode for microbial fuel cells. *Energy* 99:193–201
12. Deng LF, Dong G, Zhang YY, Li DN, Lu T, Chen Y, Yuan HR, Chen Y (2019) Lysine-modified TiO<sub>2</sub> nanotube array for optimizing bioelectricity generation in microbial fuel cells. *Electrochim Acta* 300:163–170
13. Cai H, Wang J, Bu YF, Zhong Q (2013) Treatment of carbon cloth anodes for improving power generation in a dual-chamber microbial fuel cell. *J Chem Technol Biotechnol* 88:623–628
14. Ci SQ, Wen ZH, Chen JH, He Z (2012) Decorating anode with bamboo-like nitrogen-doped carbon nanotubes for microbial fuel cells. *Electrochem Commun* 14:71–74
15. Yang Y, Liu TY, Zhu X, Zhang F, Ye DD, Liao Q, Li Y (2016) Boosting power density of microbial fuel cells with 3D nitrogen-doped graphene aerogel electrode. *Adv Sci* 3:1600097
16. Xie X, Ye M, Hu LB, Liu N, McDonough JR, Chen W, Alsharief HN, Criddle CS, Cui Y (2012) Carbon nanotube-coated macroporous sponge for microbial fuel cell electrodes. *Energy Environ Sci* 5:5265–5270



17. Xie X, Yu GH, Liu N, Bao ZN, Criddle CS, Cui Y (2012) Graphene sponges as high-performance low-cost anodes for microbial fuel cells. *Energy Environ Sci* 5:6862–6866
18. Xie X, Hu LB, Pasta M, Wells GF, Kong DS, Criddle CS, Cui Y (2011) Three-dimensional carbon nanotube-textile anode for high-performance microbial fuel cells. *Nano Lett* 11:291–296
19. Yong YC, Dong XC, Chan-Park MB, Song H, Chen P (2012) Macroporous and monolithic anode based on polyaniline hybridized three-dimensional graphene for high-performance microbial fuel cells. *ACS Nano* 6:2394–2400
20. Wang H, Wang G, Ling Y, Qian F, Song Y, Lu X, Chen SW, Tong Y, Li Y (2013) High power density microbial fuel cell with flexible 3D graphene-nickel foam as anode. *Nanoscale* 5:10283–10290
21. Lu M, Qian Y, Yang C, Huang X, Li H, Xie X, Huang L, Huang W (2016) Nitrogen-enriched pseudographitic anode derived from silk cocoon with tunable flexibility for microbial fuel cells. *Nano Energy* 32(Complete):382–388.
22. Yuan Y, Zhou S, Liu Y, Tang J (2013) Nanostructured macroporous bioanode based on polyaniline-modified natural loofah sponge for high-performance microbial fuel cells. *Environ Sci Technol* 47:14525–14532
23. Chen SL, He GH, Liu Q, Harnisch F, Yan Zhou, Chen Y, Hanif M, Wang SQ, Peng XW, Hou HQ, Schroder U (2012) Layered corrugated electrode macrostructures boost microbial bioelectrocatalysis. *Energy Environ Sci* 5:9769–9772
24. Bian B, Shi D, Cai XB, Hu MJ, Guo QQ, Zhang CH, Wang Q, Sun XLA, Yang J (2018) 3D printed porous carbon anode for enhanced power generation in microbial fuel cell. *Nano Energy* 44:174–180
25. Zhao S, Li Y, Yin H, Liu Z, Luan E, Feng Z, Tang Z, Liu S (2015) Three-dimensional graphene/Pt nanoparticle composites as free-standing anode for enhancing performance of microbial fuel cells. *Sci Adv* 1:e1500372–e1500372
26. Zhang J, Wang G, Liao ZQ, Zhang PP, Wang FX, Zhuang XD, Zschech E, Feng XL (2017) Iridium Nanoparticles Anchored on 3D graphite foam as a bifunctional electrocatalyst for excellent overall water splitting in acidic solution. *Nano Energy* 40:27–33
27. Chen LY, Li YZ, Yao JN, Wu GM, Yang B, Lei LC, Hou Y, Li ZJ (2019) Fast expansion of graphite into superior three-dimensional anode for microbial fuel cells. *J Power Sources* 412:86–92
28. Guo K, Freguia S, Dennis PG, Chen X, Donose BC, Keller J, Gooding JJ, Rabaey K (2013) Effects of surface charge and hydrophobicity on anodic biofilm formation, community composition, and current generation in bioelectrochemical systems. *Environ Sci Technol* 47:7563–7570
29. Santoro C, Guilizzoni M, Baena JC, Pasaogullari U, Casalegno A, Li B, Babanova S, Artyushkova K, Atanassov P (2014) The effects of carbon electrode surface properties on bacteria attachment and start up time of microbial fuel cells. *Carbon* 67:128–139
30. Bi LL, Ci SQ, Cai PW, Li H, Wen ZH (2018) One-step pyrolysis route to three dimensional nitrogen-doped porous carbon as anode materials for microbial fuel cells. *Appl Surf Sci* 427:10–16
31. Wu XS, Qiao Y, Shi ZZ, Tang W, Li CM (2018) Hierarchically porous N-doped CNTs/peduced graphene oxide composite for promoting flavin based interfacial electron transfer in microbial fuel cells. *ACS Appl Mater Inter* 10:11671–11677
32. Mohamed HO, Sayed ET, Cho H, Park M, Obaid M, Kim H-Y, Barakat NAM (2018) Effective strategies for anode surface modification for power harvesting and industrial wastewater treatment using microbial fuel cells. *J Environ Manag* 206:228–235
33. Kim JR, Cheng SA, Oh SE, Logan BE (2007) Power generation using different cation, anion, and ultrafiltration membranes in microbial fuel cells. *Environ Sci Technol* 41:1004–1009
34. Zhao CE, Li JX, Chen Y, Chen JY (2019) Nitrogen and sulfur dual-doped graphene as an efficient metal-free electrocatalyst for the oxygen reduction reaction in microbial fuel cells. *New J Chem* 43:9389–9395
35. Bard AJ, Faulkner LR (2001) *Electrochemical methods: fundamentals and applications*, 2nd edn. Wiley, New York
36. Qiao Y, Li CM, Bao SJ, Bao QL (2007) Carbon nanotube/polyaniline composite as anode material for microbial fuel cells. *J Power Sources* 170:79–84
37. Banks CE, Davies TJ, Wildgoose GG, Compton RG (2005) Electrocatalysis at graphite and carbon nanotube modified electrodes: edge-plane sites and tube ends are the reactive sites. *Chem Commun* 7:829–841
38. Ci SQ, Cai PW, Wen ZH, Li J (2015) Graphene-based electrode materials for microbial fuel cells. *Sci China Mater* 58:496–509
39. Lau CL, Moehlenbrock MJ, Arechederra RL, Falase A, Garcia K, Rincon R, Minter SD, Banta S, Gupta G, Babanova S, Atanassov P (2015) Paper based biofuel cells: Incorporating enzymatic cascades for ethanol and methanol oxidation. *Int J Hydrogen Energy* 40:14661–14666
40. Feng CH, Ma L, Li FB, Mai HJ, Lang XM, Fan SS (2010) A polypyrrole/anthraquinone-2,6-disulphonic disodium salt (PPy/AQDS)-modified anode to improve performance of microbial fuel cells. *Biosens Bioelectron* 25:1516–1520

**Publisher's Note** Springer Nature remains neutral with regard to jurisdictional claims in published maps and institutional affiliations.